To be submitted for publication

Simulation of redistributive and erosive effects in a-Si under Ar^+ irradiation

A. Lopez-Cazalilla,* A. Ilinov, L. Bukonte, and K. Nordlund
Department of Physics, P. O. Box 43, FIN-00014 University of Helsinki, Finland

F. Djurabekova
Helsinki Institute of Physics and Department of Physics, P. O. Box 43, FIN-00014 University of Helsinki, Finland

S. Norris
Department of Mathematics, Southern Methodist University, Dallas, Texas 75205, USA

J. C. Perkinson
Harvard School of Engineering and Applied Sciences, Cambridge, Massachusetts 02138, USA

(Dated: November 16, 2017)

Ion beams are frequently used in industry for composition control of semiconducting materials as well as for surface processing and thin films deposition. Under certain conditions, low- and medium energy ions at high fluences can produce nanoripples and quantum dots on the irradiated surfaces. In the present work, we focus our attention on the study of irradiation of amorphous silicon (a-Si) target with 250 eV and 1 keV Ar^+ ions under different angles, taking into special consideration angles close to the grazing incidence. We use the molecular dynamics (MD) method to investigate how much the cumulative displacement of atoms due to the simulated ion bombardment contribute to the patterning effect. The MD results are subsequently analysed using a numerical module Pycraters that allows the prediction of the rippling effect. Ripple wavelengths estimated with Pycraters are then compared with the experimental observations, as well as with the results obtained by using the binary collisions approximation (BCA) method. The wavelength estimation based on the MD results demonstrates a better agreement with the experimental values. In the framework of the utilized analytical model, it can be mainly attributed to the fact that the BCA ignores low energy atomic interactions, which, however, provide an important contribution to the displacement of atoms following an ion impact.

I. INTRODUCTION

Low- and medium-energy ion beam irradiation is an industrial tool widely used for material processing, e.g. doping, sub-lithographic nano-fabrication or surface polishing. Ion irradiation of semiconductor surfaces can result in formation of various periodically ordered nano and micro structures, such as dots or ripples[1–4].

The ion-induced surface pattern formation phenomena is conventionally described by the Bradley-Harper theory[5]. This theory is based on the curvature dependence of the sputtering yield, and reasonably explains the mechanisms that lead to pattern formation under the off-normal incidence conditions. However, the original theory is not able to predict the transition from the parallel mode ripples which appear when the ion beam is closer to the normal incidence (but always beyond some critical angle), to the perpendicular mode ripples appearing close to the grazing incidence[6]. In addition, the role of the stress accumulating in the amorphous layer during the irradiation process is not well understood yet.

In most nonmetal materials, the irradiation process results in amorphization of the surface layer. This change in the material over time can be divided into two contributions. During the initial phase a prompt effect $P[x]$ is related to those atoms that are displaced and reach the surface with enough energy to be sputtered (erosive part), and also to the atoms displaced within the solid (redistributive). This phase takes place within the timescale of up to 10^{-12} s. Effects noted at longer time scales are included in the gradual relaxation part $G[x]$. Both effects together contribute to the rate of motion of the surface v_n,

$$v_n = P[x] + G[x]. \tag{1}$$

In order to quantify the contribution of the prompt effect $P[x]$, a new method of analysing the collective motion of individual atoms was developed in 2011[7] using the molecular dynamics (MD). This method provides more precise information regarding the pattern formation than the binary collision approximation (BCA), due to the ability to capture small atomic displacements demonstrated by Bukonte et al.[8]. Nevertheless, complex subtraction of background displacements was needed due to the presence of residual stresses in the simulated sample[7]. In this work we present a new relaxation method which prepares the amorphous target in such a way, that subtraction of background effects becomes unnecessary for an accurate analysis of ion-induced displacements.

II. METHODS

Study of mechanisms leading to ripple formation on a-Si surfaces is done using the PARCAS MD code[9,10] and CASWIN BCA code[11]. Both methods have been used to analyse sputtering and measure atomic displacements in the a-Si target.

MD is a deterministic computational technique which reproduces the evolution of a set of atoms by solving the equations of motion iteratively starting from a given distribution of atom coordinates and velocities. BCA, on the other hand, is a Monte Carlo type stochastic algorithm that solves scattering integral for each collision. The impact parameter to the next collision is chosen randomly and depends on the density of the target. In contrast to MD, BCA treats the full atomic dynamics of a material by a series of binary collisions neglecting many body interactions and, therefore, is computationally more efficient method to study high energy cascades. Limitations and characteristic parameters of BCA are discussed later in this article.

A. Molecular Dynamics

In the case of MD, the environment-dependent interatomic potential (EDIP) for bulk Si[12,13] is used. This potential is able to provide a realistic model of the amorphous structure regarding the density and the coordination number. Before launching simulations of ion irradiation process, the a-Si cell is prepared and thoroughly relaxed as described in the Section II A 1.

1. Cell Construction and Relaxation

The initial system is an a-Si 40x40x10 nm^3 (877952 atoms) rectangular cuboid with periodic boundaries, composed by replication from the smaller 10x10x10 nm^3 a-Si cell previously generated using the Wooten-Winer-Weaire (WWW) method[8,14]. The WWW method is capable of creating an amorphous structure free of coordination defects, but is computationally expensive. The 40x40x10 nm^3 a-Si structure has been equilibrated at 300 K with the Berendsen temperature and pressure controls[15] to reduce the normal components of the internal stress; the time constant of the Berendsen algorithm was set to 500 fs. The system size was fixed and the system has subsequently been annealed by repeatedly heating up to 1000 K (corresponding to the glass transition temperature of a-Si[16]) and linearly cooling down to 300 K during 50 ps for each of 20 iterations to optimize the structure. After the annealing stage, the system temperature has been linearly decreased from 300 K to 0 K during 50 ps with the pressure control enabled to obtain the size of the relaxed cell at 0 K. Up to this point x,y and z directions have always been periodic. The system size in x and y directions had been fixed and stayed intact during all of the following steps.

To prepare a bigger target for more realistic cooling conditions and to prevent a possible shock wave reflection, the initial a-Si cuboid has been replicated three times along the periodic x-direction. To simulate an open surface of an infinitely large sample, periodicity has been disabled for the z direction; at the same time it stayed enabled for the x and y directions. The system with an open surface has been simulated for 50 ps at 300 K to relax the surface, and subsequently cooled down to 0 K using the Berendsen temperature control for 15 ps, which was enough to lead the system temperature to ≈ 0.001 K and hence minimize the thermal motion of Si atoms. Irradiations are performed across the XY upper surface and several atomic layers at the bottom are immobilized in order to prevent the movement of the system.

The evolution of the system during the last cooling stage is shown in Fig. 1. The final pressure is not zero because the top surface of the cell is open, hence the surface tension contributes to the total pressure in the cell.

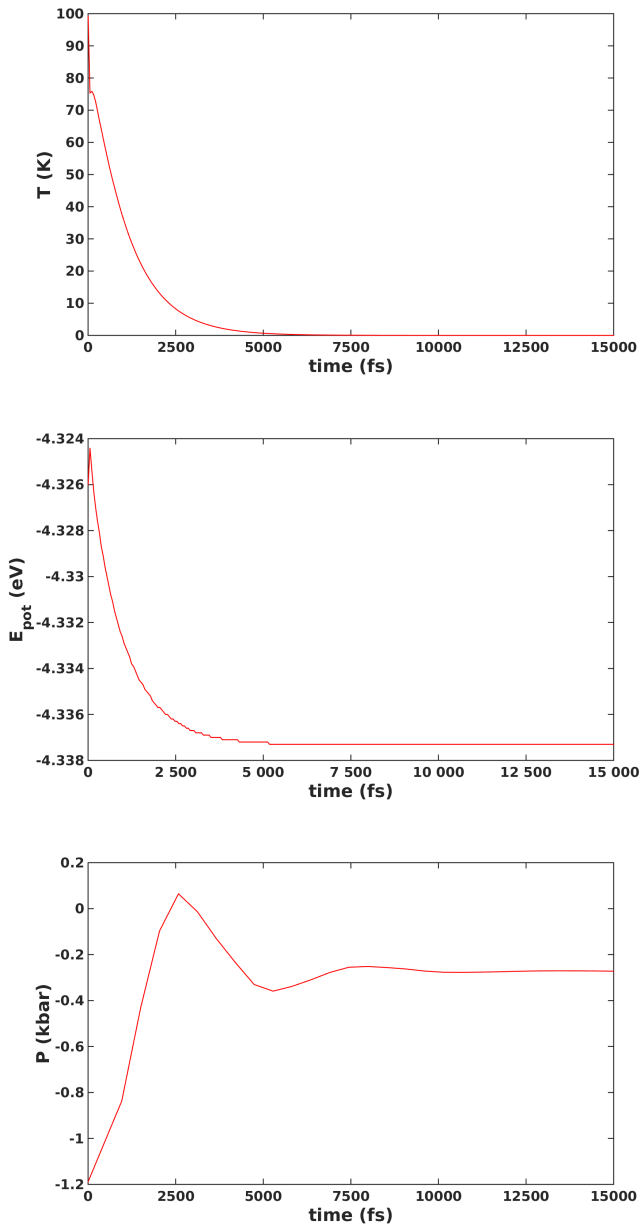

FIG. 1: Evolution of the system during the relaxation process.

The construction and relaxation of the amorphous sample is one of the key stages of this work. In the previous study[7] a complex process of background subtraction was necessary to exclude small displacements which appeared after ion impacts, but were not directly attributed to the redistributive effect. Such displacements did not depend on the azimuthal angle of the incoming ion, and originated from atomic movement in zones which had large unrelaxed residual stresses; the stresses were unintentionally relaxed due to an extra energy transmitted from incoming ions during collision cascades. In the current work, the success of the relaxation stage is analysed, firstly, by measuring residual displacements when simulating the system in similar conditions as during irradiation, but when no actual ion bombardment is performed. The analysis has demonstrated that only 12 atoms out of 2.6 million in the system had a displacement greater than 0.01 nm during 50 ps simulation; the distribution of kinetic energies of atoms corresponded to the system temperature of 0.001 K. The averaged (background) displacement of atoms after impacts performed with random azimuthal angles was of a similar order, and about two orders of magnitude smaller than displacements during a typical individual irradiation event. In addition, the analysis of shear displacements in the system, done similarly as in[7], demonstrated no distinguishable shear effect of ion impacts. Taking everything into account, it can be concluded that the system is sufficiently relaxed and the selected system size and relaxation times allows for a direct measurement of ion induced atomic redistribution.

2. *Irradiation*

The a-Si target is bombarded with either 250 eV or 1 keV Ar^+ ions, positioned at the 1 nm distance above the surface in the beginning of every simulation. The irradiation is performed at different incidence angles in the range of $0° - 88°$, in such a way the ion is always in the geometrical center of the surface. Each irradiation run was repeated 600 times for 1 keV (300 times for 250 eV) utilizing the approach of a random cell shift along the periodic directions prior to each ion impact, using a random number multiplied by the dimension of the cell, Δs_x and Δs_y, respectively. This approach allows to introduce the incoming ion always in the center of the cell, while the atomic environment changes, corresponding to the random impact position. Then Δs_x and Δs_y are used to relocate the atoms through the boundaries of the cell in x and y directions. After several test runs, we have verified that atomic displacements due to ion impacts on average do not propagate further than 10 nm from the initial impact point.

In order to get better statistics, we continue to perform simulations with random azimuthal angles. The simulation time for every irradiation event is 50 ps, assuring the simulation is long enough to collect all the atomic displacements.

The bottom layer (1 nm thick) of the cell is fixed to prevent the system motion. During all irradiation simulations, the Berendsen thermostat with the time constant of 50 fs and the target temperature of 0 K is applied to a 0.5 nm thick region along the borders of the cell, except the upper open surface, to resemble the cooling conditions of a bulk sample. After the 50 ps irradiation simulation, the Berendsen thermostat is applied for all atoms in the system during the 5 ps cooling stage with the time constant of 500 fs, to eliminate the remaining thermal motion.

The Ar interaction with the Si target is described by

the purely repulsive interatomic potential calculated using the density functional theory method with a numerical basis sets for Ar-Si dimer by Nordlund et al.[17]. The same method was used to create Si-Si short-range repulsive potential, which was smoothly joined to the EDIP potential at short distances to correctly represent high energy Si-Si atomic collisions.

In the following sections, we compare our results with the previous results of Norris et al. on 250 eV Ar^+ to a-Si single-ion irradiation[7].

B. Binary Collisions Approximation

The simulations are performed using the CASWIN code[11], in which the target is considered to be amorphous. In CASWIN, atomic collisions are calculated at every step of a projectile (moving atom) at the distance of a mean free path ($\lambda = n_a^{-1/3}$, where n_a is the atomic density) from the previous position in the direction after scattering. The MAGIC formula[18] is used as an approximation of the scattering integral calculated with the Coulomb potential screened by the function proposed by Ziegler, Biersack and Littmark[19] in order to treat the collisions. The validity of the CASWIN code was tested previously against the MD simulations, see Ref. 20 and 21. In the former work, we obtained very close agreement in ion range profiles for Si ions in amorphous Si matrix (CASWIN) and polycrystalline Si (MDRANGE[22]) by using the same atomic density and the ZBL potential.

In these simulations we assume the surface region (0.5 nm) to be different from the bulk. In the surface region, the cut-off energy and the displacement threshold energy are considerably lower than in the bulk and, the latter, corresponds approximately to the surface energy. The BCA considers only atoms that have kinetic energy above the cut-off value, hence we chose the cut-off energies of 3 eV and 1 eV for bulk and surface simulations, respectively. The threshold displacement energy, or a minimum energy for an atom to be displaced permanently from its position, is the parameter determining the damage production in the BCA simulation. We chose this value to be 13 eV[8]. The sputtering process is defined by the surface binding energy of 4.7 eV.

In Table I, we summarize all the parameters used in our simulations to obtain the atomic displacements in collisional cascades within the binary collision approximation; these parameters are directly taken from [8].

TABLE I: Parametrization of BCA simulations[8].

Parameter(unit)	
Density (N/Å^3)	0.05340
Threshold displacement energy (eV)	13
Surface binding energy (eV)	4.7
Surface cut-off energy (eV)	1.0
Bulk cut-off energy (eV)	3.0

C. Analysis

In order to predict the pattern formation, we solve the partial differential equation (PDE) describing the evolution of the surface using the crater function equation:

$$\frac{\partial h(x,y,t)}{\partial t} = \left(S_X(\theta)\frac{\partial^2 h}{\partial x^2} + S_Y(\theta)\frac{\partial^2 h}{\partial y^2} \right) - B\nabla^4 h, \quad (2)$$

where θ is the irradiation angle, B is a viscous flow coefficient obtained from experiments, and h is the height of a certain point at the surface. The angle-dependent coefficients $S_X(\theta)$ and $S_Y(\theta)$ are defined including the effect of the curvature explained by Harrison et al.[23]:

$$\begin{aligned} S_X(\theta) &= \frac{d}{d\theta}[M^{(1)}(\theta)\cos(\theta)] + \cos(\theta)\frac{\partial}{\partial K_{11}}M^{(0)}(\theta)\Big|_{K_{11}=0} \\ S_Y(\theta) &= M^{(1)}(\theta)\cos(\theta)\cot(\theta) + \cos(\theta)\frac{\partial}{\partial K_{22}}M^{(0)}(\theta)\Big|_{K_{22}=0}, \end{aligned} \quad (3)$$

where I_0 is the flux, $K_{11} = \frac{\partial^2 h}{\partial x^2}(0,0)$ and $K_{22} = \frac{\partial^2 h}{\partial y^2}(0,0)$. Those coefficients are calculated from the first moments of the crater function obtained from either MD or BCA simulations. According to the surface stability model developed by Norris et al[24], the ripple formation can be predicted if two components of the crater function are determined. Using PyCraters[25] we can calculate the coefficients from the moments, but in the case of the second term in the right part of the Eq.(3), an approximation related to the Sigmund ellipsoidal model of erosion[23,26] is used to estimate those. In order to calculate these coefficients we consider two parts: erosive, which is dependent on the number of sputtered atoms, and redistributive, which depends on the movement of the non-sputtered atoms:

$$\begin{aligned} M^{(0)}_{\text{erosive}} &= -V_{\text{Si}} \sum_{j=1}^{N_{\text{sputt}}} 1 \\ M^{(1)}_{\text{erosive}} &= -V_{\text{Si}} \sum_{j=1}^{N_{\text{sputt}}} \boldsymbol{u}_j^{\text{initial}}, \end{aligned} \quad (4)$$

$$\begin{aligned} M^{(0)}_{\text{redist.}} &= 0 \\ M^{(1)}_{\text{redist.}} &= V_{\text{Si}} \sum_{j=1}^{N_{\text{red}}} (\boldsymbol{u}_j^{\text{final}} - \boldsymbol{u}_j^{\text{initial}}), \end{aligned} \quad (5)$$

where N_{sputt} and N_{red} represents the total number of sputtered and redistributed atoms in the sample, respectively; V_{Si} is the atomic volume of Si atoms, and $\boldsymbol{u}_j = (x_j, y_j)$ are the atomic coordinates before or after an ion impact. To make the analysis simpler, atomic

coordinates have been transformed to a local coordinate system associated with the surface normal and the projected ion beam direction, with the origin in the ion impact point. This way the projected ion beam is always directed along the x axis of the local coordinate system, so on average the y components of $M^{(1)}_{\text{redist.}}$ and $M^{(1)}_{\text{erosive}}$ are expected to be zero. Conversion to a local coordinate system was done according to the rotation transformation equations:

$$\begin{aligned} x_j &= x_j^{'}\cos(\phi) + y_j^{'}\sin(\phi) \\ y_j &= -x_j^{'}\sin(\phi) + y_j^{'}\cos(\phi), \end{aligned} \tag{6}$$

where ϕ is the azimuthal angle of the incoming ion and $(x_j^{'}, y_j^{'})$ are the original coordinates of the atoms in the system related to the simulation cell.

III. RESULTS AND DISCUSSION

We present the moments of the crater function extracted from both MD and BCA simulations by using Eqs. (4) and (5) separately in sections III 1 and III 2 for both types of simulations. These moments are used to obtain the coefficients S_x and S_y (see Eq.(3)), which are in turn applied for the prediction of the ripple formation.

1. S_x and S_y moments from MD simulations

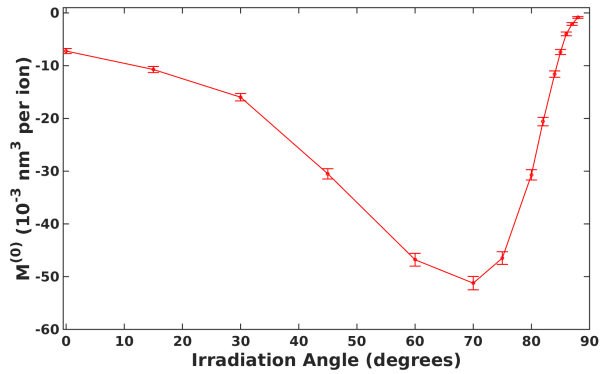

(a)

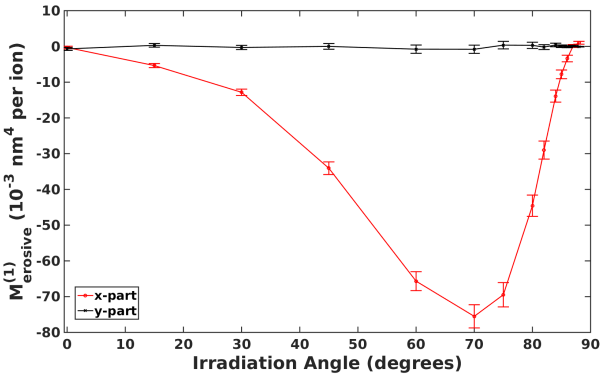

(b)

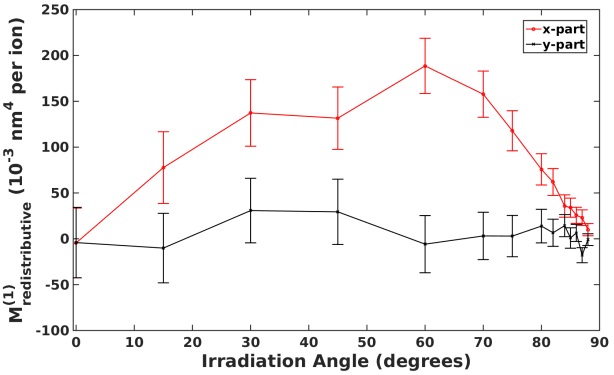

(c)

FIG. 2: Average moments of the crater function from MD under 1 keV Ar^+ irradiation as a function of the incidence angle. (a) Zeroeth Moment $M^{(0)}$. (b) First erosive moment $M^{(1)}_{\text{erosive}}$. (c) First redistributive moment $M^{(1)}_{\text{redist.}}$. One σ confidence intervals are represented in the error bars (68.2 %).

Moments, extracted from the results of MD simulations are shown in Fig. 2. The coefficients $S_x(\theta)$ and $S_y(\theta)$ are then calculated according to the Eq. (3). To do

that, the crater function moments obtained from the simulation results are fitted to the Fourier series, defined by the symmetry conditions and the fact that all moments are approaching zero at the grazing incidence. This provides a continuous interpolation of the moment values for all incidence angles in the 0 - 90 degrees range. Uncertainties in $S_x(\theta)$ and $S_y(\theta)$ coefficients are estimated through the linear approximation of the error propagation theory, implemented in the package Uncertainties[27]. The calculated coefficients are demonstrated in Fig. 3.

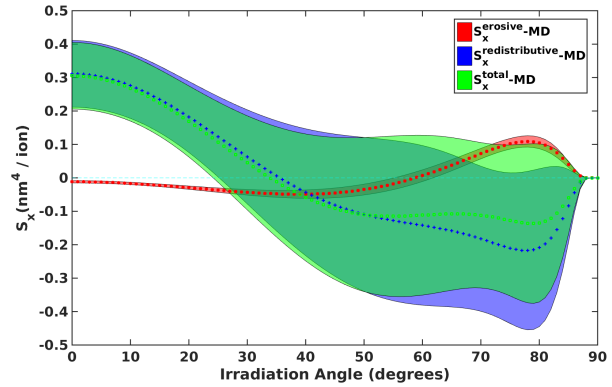

(a)

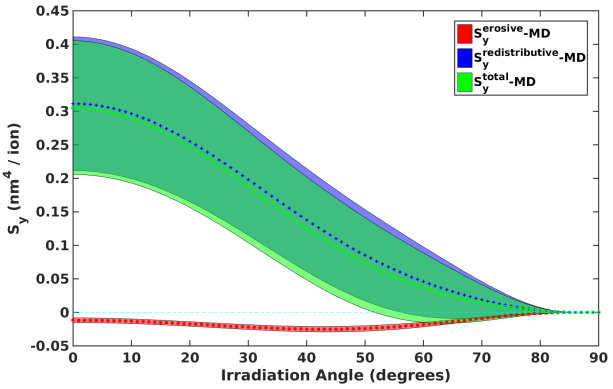

(b)

FIG. 3: MD results for 1 keV Ar^+ irradiation: (a) Coefficient $S_x(\theta)$. (b) Coefficient $S_y(\theta)$. Shaded regions represent one σ confidence intervals (68.2 %).

2. S_x and S_y moments from BCA simulations vs MD

Results obtained from the BCA simulations are shown in Fig. 4 where they are compared with the MD results. Only the x component is demonstrated , since the symmetry of the simulated geometry inevitably reduces the y component to zero. We note that this component quickly approaches zero in both MD and BCA simulations with increase of the number of statistical runs.

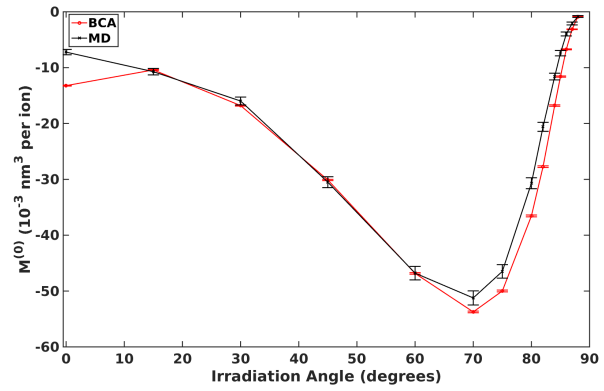

(a)

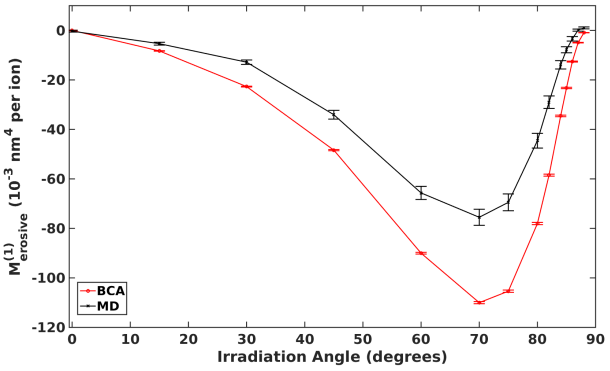

(b)

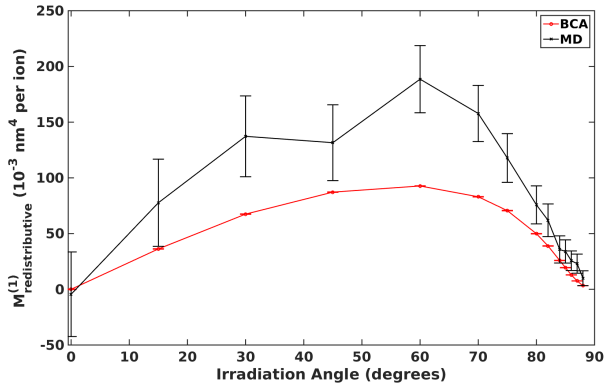

(c)

FIG. 4: Average moments of the crater function for MD and BCA as a function of the incident angle, 1 keV Ar^+ on a-Si. (a) Zeroeth Moment $M^{(0)}$. (b) First erosive moments $M^{(1)}_{\text{erosive}}$. (c) First redistributive moments $M^{(1)}_{\text{redist.}}$.

It is noticeable in Fig. 4 that although the zeroeth erosive moments (proportional to the number of sputtered atoms) agree quite well for both methods, there is a larger disagreement between the first erosive moments. It means that atoms which are ejected from the surface in MD simulations are on average closer to the impact point than in BCA. This could be explained by

the fact that sputtering occurs at the final stages of the collision cascade evolution, when colliding atoms already have such a low energy that many-body interactions considered in MD, but ignored in BCA, become important for a reliable trajectory prediction. We had analysed the kinetic energy of sputtered atoms for 1keV Ar^+ irradiation at 70° off-normal and found that indeed majority of the sputtered atoms had the energy well below 50 eV (Fig. 5).

In the manuscript[28] the authors demonstrate that at such energies the BCA method overestimates penetration depths of ions for the non-channelling directions in comparison with the MD.

This difference in the first erosive moment makes the erosive component of S_x to be significantly different between MD and BCA for the higher incidence angles, though the sputtering yields remain similar (Figs. 3 and 6)

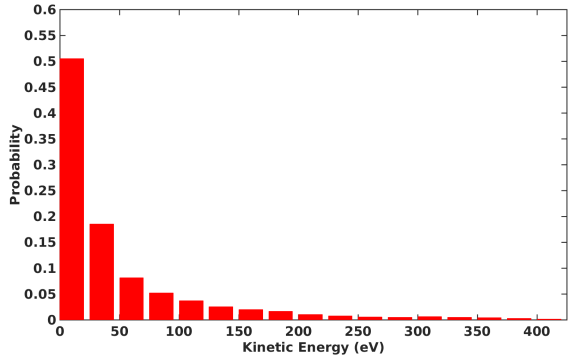

FIG. 5: Kinetic energy distribution of sputtered atoms for 1 keV Ar^+ on a-Si at 70^o off-normal in MD.

The coefficients $S_x(\theta)$ and $S_y(\theta)$ for the BCA simulations are calculated using the obtained moments of the crater function. These coefficients are presented in Fig. 6 for 250 eV and 1 keV simultaneously, in order to demonstrate how the ion energy affects the erosive and redistributive contributions. It can be concluded that when the ion energy is increased to 1 keV, the redistributive component clearly starts to dominate at angles below 30°, whereas for the higher angles its increase is compensated by the enhanced erosive component.

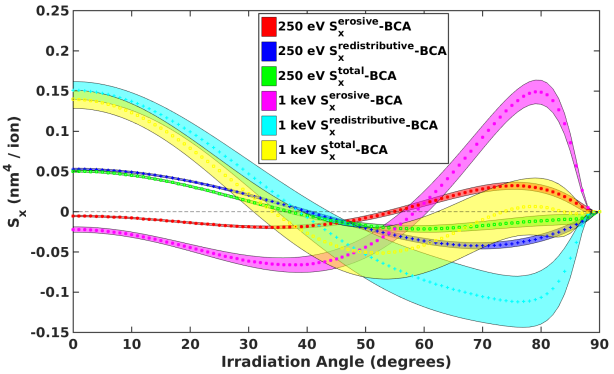

(a)

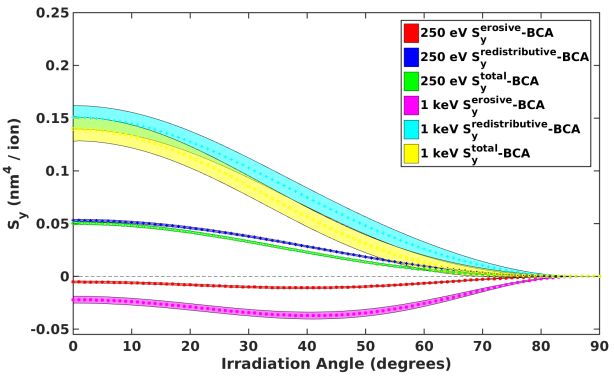

(b)

FIG. 6: BCA results for 250 eV and 1 keV Ar^+ irradiation: (a) Coefficient $S_x(\theta)$. (b) Coefficient $S_y(\theta)$. Shaded regions represent one standard error (68.2 %) confidence intervals, dotted lines highlight the mean.

In order to estimate the pattern wavelength, we need the coefficients S_x, S_y, calculated in Section II C. The relative accuracy of S_x coefficients (which define the parallel-mode ripples) is evaluated by comparing with the values of S_x obtained from the amplification factor equation by Madi et al.[29]:

$$R(\boldsymbol{q}) = -S_x q_x^2 - S_y q_y^2 - B(q_x^2 + q_y^2)^2 \qquad (7)$$

where the values of $R(\boldsymbol{q})$ are measured experimentally.

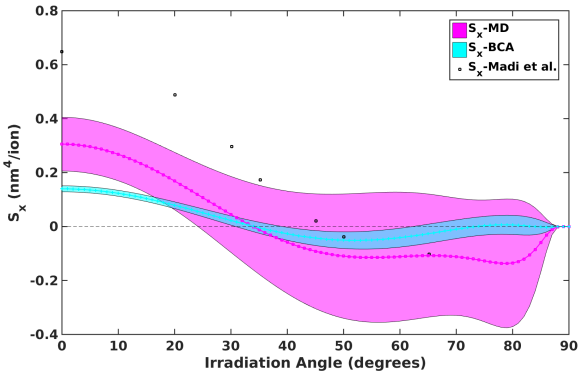

FIG. 7: Comparison between MD and BCA for 1 keV Ar^+ on a-Si of coefficient $S_x(\theta)$. Shaded regions represent one σ confidence intervals (68.2 %), dotted lines represent the mean.

Fig. 7 demonstrates how well the MD and BCA results agree with the experimental data. From the normal incidence to 35^o both methodologies clearly underestimate the value of the S_x coefficient; for the higher incidence angles the agreement becomes better as the coefficient approaches the destabilizing region with the negative S_x values. The reason for the difference between the MD and BCA results at the smaller angles can be mainly attributed to the fact that in the MD simulations the redistributive component has almost a twice larger magnitude, which is discussed in more details at the end of this section.

Additionally, in order to compare the consistency of our results with the previous simulations, the data from the work of Norris et al.[7] is plotted alongside with the new calculations for 250 eV Ar^+ ions in Fig. 8.

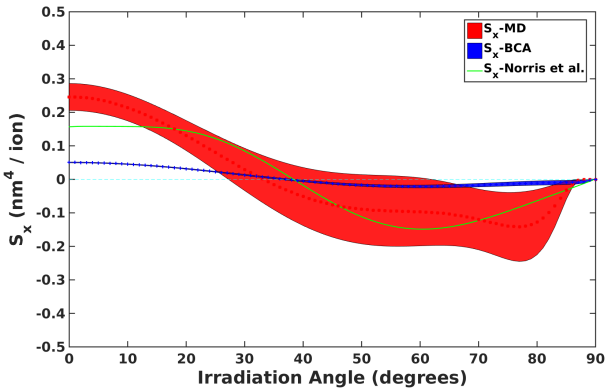

(a)

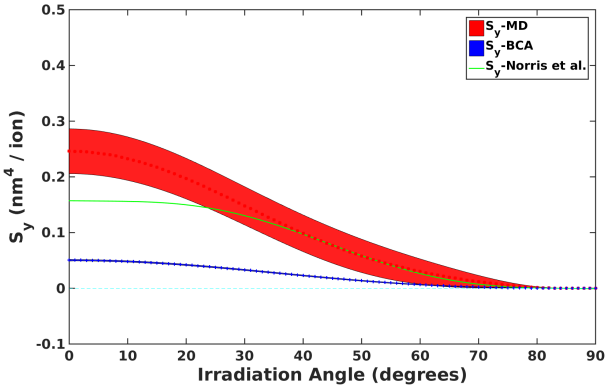

(b)

FIG. 8: Comparison between MD (own results and Norris et al.[7] results) and BCA for 250 eV Ar^+ on a-Si. (a) Coefficient $S_x(\theta)$. (b) Coefficient $S_y(\theta)$. Shaded regions represented one σ confidence interval (68.2 %), dotted lines represent the mean.

We see that both MD results are larger in magnitude than the BCA ones due to larger contribution of the redistributive part. Besides, a slight difference is observed also between both MD results. One possible explanation is that the a-Si samples have been prepared differently, and the collected statistics is not sufficient for more accurate evaluation of the crater function moments. Another reason for the difference can be due to the geometry of the regions taken into consideration. In the present work, the whole cell (with the exception of the thermal bath region) is used to perform the displacement analysis; on the other hand, Norris et al. used the region within a radius of 7.5 nm from the impact point. The result might vary due to the influence of small displacements occurring far from the impact point, even though the relaxation performed is sufficient. To verify that, we perform test simulations with an a-Si target of even larger size, having dimensions of 60 nm x 60 nm x 30 nm. It turns out that on average the contribution of displacements further than 10 nm from the impact point is negligible in the total value.

Once the coefficients are calculated, the ripple wavelength can be estimated from Eq. (2) using the following expression:

$$\lambda(\theta) = 2\pi\sqrt{\frac{2B}{-fS_{x,y}(\theta)}}, \tag{8}$$

where the viscous flow coefficient B is estimated from the experimental results[7,29] and f is the flux. The criteria used to choose either the parallel (S_x) or the perpendicular coefficient (S_y), is the most negative (unstable) one. In case of both coefficients being non-negative, a surface instability will not appear. Using a value for $B = 0.062$ nm^4 s^{-1}, a comparison can be done between the BCA and the MD methodologies.

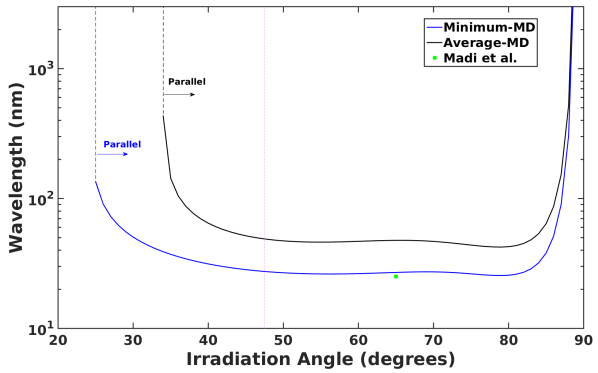

(a)

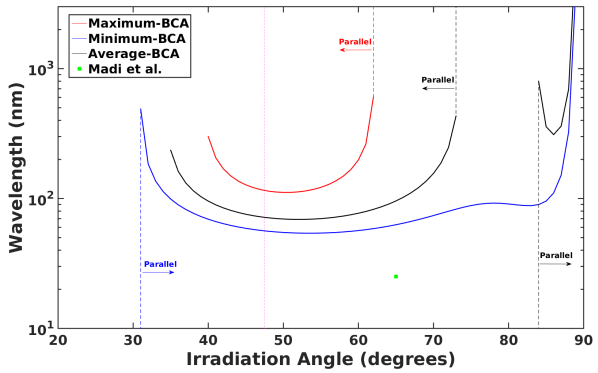

(b)

FIG. 9: Predicted ripple wavelength for MD and BCA for 1 keV Ar^+ on a-Si, after applying a flux of f = 2.0×10^{12}cm^{-2}s^{-1} using the mean, the lower and the upper error boundary estimations for S_x and S_y coefficients shown in Fig. 7. The magenta vertical dotted line indicate the experimental critical angle. The green dot represent the experimental point measured by Madi et al.[29]

In Fig. 9, the wavelength predicted according to Eq. (8) is plotted for both methods using the mean value and both the lower and the upper confidence bounds of $S_x(\theta)$ and $S_y(\theta)$ coefficients. As can be observed from the plot, MD results show that surface rippling is predicted from about 34^o off-normal angle on average, which differs from the experimental value of the critical angle, but this value changes when the wavelength calculation is done using the minimum estimation to 25^o. According to the mean and the lower confidence bounds, for the whole range of irradiation angles where a pattern appears, the parallel mode ripples are predicted due to the dominance of $S_x(\theta)$ component. Nevertheless, for the upper confidence bound no rippling is predicted, because, according to the model, a negative value of $S_{x,y}$ is needed to observe a surface instability, and for positive $S_{x,y}$ the wavelength is not defined.

Looking at the BCA calculations, an identical behaviour is observed for the lower bound prediction, where parallel mode ripples appear from 31^o, and the upper boundary estimation predicts ripples to become parallel from 40^o to 62^o. However, according to the mean value estimation, rippling is predicted from 35^o, differing with the experimental results. Besides, a discontinuity (meaning stable surface height) appears between 74^o and 83^o as a result of the positive values of both $S_x(\theta)$ and $S_y(\theta)$ in this range.

Moreover, comparing the experimental data by Madi et al.[29] with our results, it can be observed that MD reproduces the wavelength more accurately, positioning MD as a better method of simulations of effects preceding surface rippling.

In the light of the results we can observe significant differences between MD and BCA. For the zeroeth moment (Fig. 4a), there is a good consistency in the average number of sputtered atoms; a sputtering maximum is observed for both methods at 70^o incidence. However, the first erosive and redistributive moments (Fig. 4b and 4c respectively) given by BCA agree much less with those extracted from the MD simulations. In general, we note that in the BCA simulations the value of the erosive component is larger in magnitude than the redistributive one, contributing stronger to the pattern formation mechanism.

In the case of the first redistributive moment, there is a clear domination of this component for MD. Although the maximum of this moment is reached in both MD and BCA simulations at 60^o, it is noticed that in MD the absolute value is greater than in BCA. This can be explained as a consequence of the type of collisions that each method takes into consideration. Those collisions which provoke small displacements are crucial for understand of the differences between both methodologies. In order to measure the contribution, the delta parameter (total displacement) can be calculated; it is defined as a sum of magnitudes of individual atomic displacements:

$$\delta = \sum_{j=1}^{N_{\rm red}} \sqrt{\Delta x^2 + \Delta y^2 + \Delta z^2}, \tag{9}$$

where $\Delta x = x_j^{\text{final}} - x_j^{\text{initial}}$; Δy and Δz are calculated similarly. It is important to note, that for both the initial and the final states the system temperature should be minimized to 0 K, otherwise the random thermal displacements will introduce inaccuracies to this calculation. The contribution to the total displacement can be calculated as a function of the sum of atomic displacements greater than a certain threshold value (r), therefore the importance of smaller displacements can be evaluated.

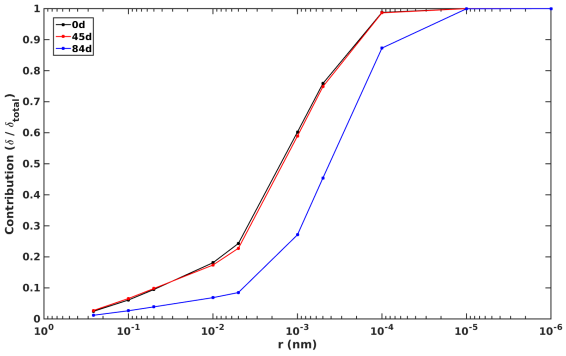

FIG. 10: Cumulative contribution to the total displacement as a function of the displacement magnitude for MD simulations, for $0, 45, 84^o$ incidence angles under 1 keV Ar^+ irradiation.

As it is showed in Fig. 10, atomic displacements larger than 0.05 nm do not contribute more than 0.1 to the total displacement. Therefore, it is important that smaller displacements are also taken into consideration, as they provide the substantial part of the total displacement. A similar behaviour has been observed by Bukonte et al. in[8].

IV. CONCLUSIONS

In this work we performed a more consistent relaxation of the a-Si target prior to ion impacts, which allowed us to avoid the complex background removal process required in the previous study[24] for reliable capturing of small scale atomic displacements. It seems that the sufficiently big target size and the after-impact relaxation times are crucial for minimization of the artificial effects, arising from the simulation setup configuration.

The results of this work confirm the dominating effect of the redistributive component of the first moment of the crater function on the predicted surface patterning under 1keV Ar^+ ion irradiation. We also verified that the model is valid at angles close to the grazing incidence. It has been demonstrated that the BCA algorithm, which takes into account only binary collisions and thus overlooks the low energy many-body interactions, may lead to the disproportional effect of the erosive component of the first moment of the crater function, thus resulting in an inaccurate prediction of the surface pattern formation.

The model by Norris et al.[24] allows us to predict the pattern wavelength originated from the ion bombardment using a mathematical model, which makes it possible to estimate this value from parallel single-ion irradiations, without performing computationally demanding high fluence consecutive irradiation simulations. The predicted wavelength, calculated using this approach is in a relatively good agreement with the experimental results.

As we have seen throughout the present work, the main difference between MD and BCA is the predicted weight of the erosive and redistributive components in the total contribution. The redistributive part is the larger contributor to the result in MD, leads us to see that MD approximates better the experimental results than BCA according to the implemented model.

ACKOWLEDGEMENTS

This work was performed within the Finnish Centre of Excellence in Computational Molecular Science (CMS), financed by The Academy of Finland and University of Helsinki. Computational resources provided by CSC, the Finnish IT Center for Science as well as the Finnish Grid and Cloud Infrastructure (persistent identifier urn:nbn:fi:research-infras-2016072533) are gratefully acknowledged.

* Corresponding author alvaro.lopezcazalilla@helsinki.fi

[1] S. Facsko, T. Dekorsy, C. Koerdt, C. Trappe, H. Kurz, A. Vogt, and H. Hartnagel, Science **285**, 1551–1553 (1999).
[2] B. Ziberi, F. Frost, T. Höche, and B. Rauschenbach, Phys. Rev. B **72**, 235310 (2005).
[3] U. Valbusa, C. Boragno, and F. Buatier de Mongeot, J. Phys.: Condens. Matter **14**, 8153 (2002).
[4] A. Cuenat, H. George, K.-C. Chang, J. Blakely, and M. Aziz, Adv. Mater. **17**, 2845 (2005).
[5] R. M. Bradley and J. M. Harper, J. Vac. Sci. Technol. **6**, 2390–2395 (1988).
[6] C. S. Madi, H. B. George, and M. J. Aziz, J. Phys. Condes. Matt. **21**, 224010 (2009).
[7] S. A. Norris, J. Samela, C. S. Madi, M. P. Brenner, L. Bukonte, M. Backman, F. Djurabekova, K. Nordlund, and M. J. Aziz, Nature communications **2**, 276 (2011).
[8] L. Bukonte, F. Djurabekova, J. Samela, K. Nordlund, S. A. Norris, and M. J. Aziz, Nucl. Instr. Meth. Phys. Res. B **297**, 23 (2013).

[9] M. Ghaly, K. Nordlund, and R. S. Averback, Phil. Mag. A **79**, 795 (1999).
[10] K. Nordlund, M. Ghaly, R. S. Averback, M. Caturla, T. Diaz de la Rubia, and J. Tarus, Phys. Rev. B **57**, 7556 (1998).
[11] F. Djurabekova, F. Umarov, and S. Yugay, IEEE **228**, 066101 (2000).
[12] M. Z. Bazant, E. Kaxiras, and J. F. Justo, Phys. Rev. B **56**, 8542 (1997).
[13] J. F. Justo, M. Z. Bazant, E. Kaxiras, V. V. Bulatov, and S. Yip, Phys. Rev. B **58**, 2539 (1998).
[14] F. Wooten, K. Winer, and D. Weaire, Phys. Rev. Lett. **54**, 1392 (1985).
[15] H. J. C. Berendsen, J. P. M. Postma, W. F. van Gunsteren, A. DiNola, and J. R. Haak, J. Chem. Phys. **81**, 3684 (1984).
[16] A. Hedler, S. L. Klaumünzer, and W. Wesch, Nature Materials **3**, 804 (2004).
[17] K. Nordlund, N. Runeberg, and D. Sundholm, Nucl. Instr. Meth. Phys. Res. B **132**, 45 (1997).
[18] J. P. Biersack and L. G. Haggmark, Nucl. Instrum. Meth. **174**, 257 (1980).
[19] J. F. Ziegler, J. P. Biersack, and U. Littmark, (Pergamon, New York) (1985).
[20] K. Nordlund, F. Djurabekova, and G. Hobler, Physical Review B **94** (2016).
[21] K. Nordlund, D. Sundholm, P. Pyykkö, D. M. Zambrano, and F. Djurabekova, Physical Review A **96** (2017).
[22] K. Nordlund, Computational Materials Science **3**, 448 (1995).
[23] M. Harrison and R. Bradley, Phys. Rev. B **89**, 245401 (2014).
[24] S. A. Norris, M. P. Brenner, and M. J. Aziz, Journal of Physics-Condensed Matter **21**, 224017 (2009).
[25] S. A. Norris, arXiv:1410.8489.
[26] P.Sigmund, J Mater Sci **8**, 1545 (1973).
[27] E. O. Lebigot, http://pythonhosted.org/uncertainties/ **V.3.0.1** (2017-04-19).
[28] G. Hobler and G. Betz, Nucl. Instr. Meth. Phys. Res. B: Beam Interactions with Materials and Atoms **180**, 203 (2001).
[29] C. S. Madi, E. Anzenberg, K. F. L. Jr., and M. J. Aziz, Phys. Rev. Let. **106**, 066101 (2011).